ELSEVIER

Journal of Hazardous Materials 46 (1996) 159–168

JOURNAL OF HAZARDOUS MATERIALS

Measurement of radiation heat flux from large scale flares

T. Bjørge[a,*], A. Bratseth[b]

[a] *SINTEF/NTH Applied Thermodynamics, Trondheim, Norway*
[b] *STATOIL, Stavanger, Norway*

Received 12 April 1994; accepted 27 January 1995

Abstract

Measurements of radiation heat flux are performed on two oil rig flares in order to estimate the capacity of the flares. One measurement series is also conducted on a flare in a gas processing unit on shore for the same purpose. The results are compared with estimates using an empirical model for radiation from flares. The measured radiation heat flux levels ranged from 0.8 to 4.2 kW/m^2, depending on the location of the measurement point and on mass flow of gas (16.9–90 kg/s), wind velocity and wind direction. All sensors were located between 120 and 150 m from the estimated flame centre of the flare, on the main platform. Comparisons between computations with an empirical model and the measurements were in reasonable agreement (− 10– + 35%). If the water content of the air is taken into considerations, the discrepancy is between −33 and −6%.

Keywords: Safety; Flare; Radiation; Measurements

1. Introduction

In hydrocarbon processing plants and on oil and gas platforms, flare systems are used as a part of the safety system. In case of an emergency situation all the gas stored on the plant/platform could be dumped to the flare system. This controls and guides the design of the flare system and the location of the flare tip in relation to the plant/platform. The location is determined by allowable radiation heat flux levels. Typical levels are 1.6 kW/m^2 for continuous exposure (permanent flare), 4.7 kW/m^2 for exposure of limited duration and 6.3 kW/m^2 for short time (less than 1 min) exposure.

The heat radiated from hydrocarbon diffusion flames are mainly due to the hot soot in these flames. The amount of soot depends on the gas composition, exit gas velocity

*Corresponding author. Tel.: +47 73 593844. Fax: +47 73 593580.

SSDI 0304-3894(95)00067-4

and surrounding air flow. In addition the orientation of the flame versus the process plant/platform is of major importance. The velocity and direction of the air flow at the gas exit determines the distance between the flame and the plant/platform.

There exists both empirical models and more advanced simulation codes for calculating the heat flux from flares. Irrespective of method used, the model/code have to be validated against measurements on large scale flares. Due to the very large capacity (up to hundreds of kg/s) of real flare system, this is easiest performed at existing process plants, oil platforms or similar. The heat radiation levels at different loads and in different positions are of great importance also from pure safety considerations at such installations. This paper reports measurements performed at one process plant and two oil/gas platforms in operation.

2. Measurements

2.1. Equipment

The radiation heat flux was measured using Medtherm 64-1-20T heat flux sensors (Schmidt-Boelter type). Each sensor has a window of CaF_2 to protect the sensor and to eliminate direct convective heat transfer. The sensors are factory calibrated and the calibration is checked before and after each measurement series. The data for the sensors are given in Table 1. The view angle of the sensors are 150° with window. Because of large distance between each measurement position and to remove the necessity of a local amplifier, each sensor is connected to a separate A/D converter through a short cable (6 m). The A/D converters are Schlumberger 35951A isolated measurement pods (IMP). These A/D converters have 20 channels [1]. In order to make the measurement equipment Ex approved, each IMP was placed in a EEx de (ia) IIC T5 housing. The IMPs are connected in series to a PC by a S-Net cable. The total cable length can be up to 1000 m. To control the IMPs, a PC to S-Net Adaptor is located in the PC [2] (Schlumberger 35954A). The voltage supply to the IMPs goes through the S-Net cable using an external voltage supply (Schlumberger 359595A).

Table 1
Data for the heat flux sensors

Model	64-1-20T
Range (kW/m^2)	0–11.342
Output (mV)	0–10
Temperature limit (°C)	200
Maximum non-linearity (%)	±2 of full scale
Repeatability (%)	±0.5
Accuracy (%)	±3
Absorbtivity	0.97 in the range 0.6–15 μm (CaF_2: 0.1–8 μm)
Response time (s)	< 1.5

The last IMP has a termination at the S-Net output to prevent reflections in the S-Net cable.

The data collection is controlled by the Altair software from Dickinson Control System Ltd. [3]. Further data analysis is performed using the Cypros software [4].

2.2. Location of measurement points

Fig. 1 shows a typical location of a radiation heat flux sensor in relation to the flare exit in a horizontal plane. The orientation angle α is the angle between the real north and platform/plant north. The distance L_0 is the total distance between the sensor and the flare exit. L is the distance between the senors and an estimated flame centre. Each sensor was directed towards the flare exit using a telescopic sight. Later the sensors were adjusted to an estimated flame centre by calculating the change of angle ($\Delta\phi$ in the horizontal plane as in Fig. 1 and $\Delta\theta$ in the vertical plane) based on wind direction, wind velocity and estimated outlet mass flow of gas. The coordinates of the flame centre was calculated using a program developed on the basis of the work carried out at Shell Thornton [5]. In Fig. 1, an assumed flame is also illustrated showing the definition of the wind angle β. The coordinates of the flare exit and sensors for the three measurement cases performed are depicted in Table 2.

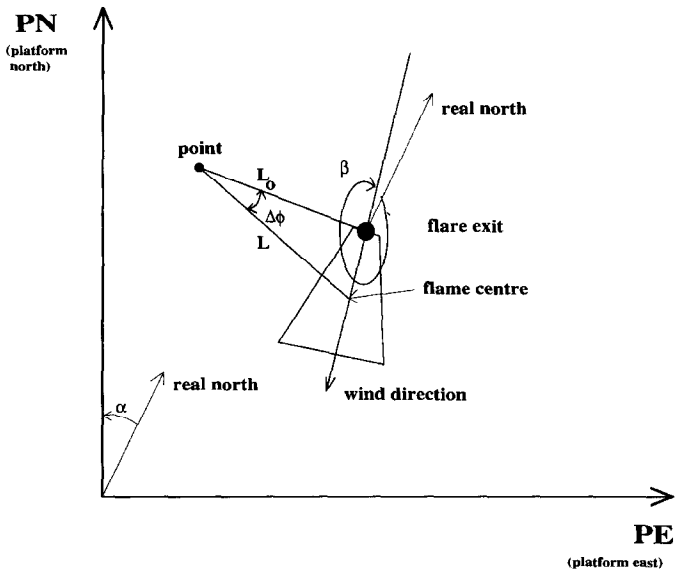

Fig. 1. A typical location of a radiation heat flux sensor and definition of relevant parameters.

Table 2
Coordinates of measurement points

Measurement series	Point #	Coordinates (m)			Orientation α (°)	Distance to flare exit L_0 (m)
		PN	PE	EL		
MI oil/gas platform	1	31.1	−89.0	−72.3		118.8
	2	5.5	−107.9	−66.1		126.7
	3	−27.4	−96.4	−74.0	23.0	124.6
	Flare exit	0.0	0.0	0.0		—
MII oil/gas platform	1	−17.0	−95.5	−64.7		116.6
	2	−33.2	−109.7	−58.7		128.8
	3	12.3	−97.1	−59.6	331.6	114.6
	4	30.3	−109.7	−58.9		128.1
	Flare exit	0.0	0.0	0.0		—
MIII gas processing plant	1	48.3	−12.9	−95.8		108.1
	2	−41.4	−25.2	−95.8		107.4
	3	35.4	35.4	−94.8		107.2
	4	−78.9	40.2	−95.8	0.0	130.5
	5	−4.6	88.5	−95.8		130.5
	6	62.6	62.6	−94.8		129.7
	Flare exit	0.0	0.0	0.0		—

2.3. *Additional data for evaluating the measurements*

In order to evaluate the measured heat flux data, additional data concerning gas composition, mass flow of gas, outlet gas temperature, outlet gas velocity, wind speed, wind direction, air temperature and relative humidity was either measured or estimated. The outlet gas velocity and outlet gas temperature were estimated from the measured mass flow and temperature in the flare knock out drum in the oil/gas platform measurements. In the gas processing plant measurements, the estimates of the same parameters were done using the measured mass flow and gas temperature in the gas pipe upstream of the flare exit. The estimated exit temperature are based on empirical correlations for flow inside pipes and past cylinders in cross flow [6].

The wind speed has to be corrected for the difference in height between the flare exit and the level of the wind data. The correction is performed using [7]:

$$\frac{\bar{u}}{v_*} = 2.5 \ln \frac{y v_*}{v} + 5.5 - 2.5 \ln\left(1 + 0.3 \frac{k v_*}{v}\right). \tag{1}$$

The value of v_* is estimated using the measured value of the mean speed at 50 m (oil/gas platforms) or 12 m (gas processing plant) height. k is the surface roughness and is taken as the wave height (MI and MII) or a typical height of disturbance of the ground (MIII).

The estimated and calculated data are shown in Table 3 for all three measurement series. In measurement series MIII, the flare system is composed of two flares. These

Table 3
Measured and calculated data for radiation heat flux measuremenrt analyses

Parameter	Measurement series			
	MI	MII		MIII
Molecular weight M (kg/kmol)	22.13	18.33	25.65	18.2 18.3 18.1
Mass flow (kg/s)	90.0 50.2	25.3 16.0	4.8 3.0	44.8 31.4 16.9
Outlet gas temperature (K)	324 322	292 292	287 287	251 255 263
Outlet diameter (m)	0.85	0.645	0.55	1.125
Outlet gas velocity (m/s)	193 107	103 65	19 12	52 37 21
Wind speed (m/s)	12.0 12.0	5.0	4.3	4.6 5.3 4.5
Wind direction (°)	35 35	280 290		262 263 259
Air temperature (K)	282	278		282
Relative humidity (%)	60	55		90

flares will later be treated as independent. The wind direction is the angle between true north and the direction the wind is coming from as depicted in Fig. 1 (β).

3. Results

Typical results of the radiation heat flux measurements are shown in Figs. 2–4 for each of the three measurement series. The sampling frequency is 1 Hz for all three series. The early peak in Fig. 3 is due to a test of the system before the flaring is started. Results of the measurements expressed as mean radiation heat flux levels and standard deviations are given in Tables 4–6 where the results also are compared with calculations. The fluctuation of the radiation heat flux level is due to the inherent turbulent behaviour of the flame and turbulent fluctuations in the approaching wind.

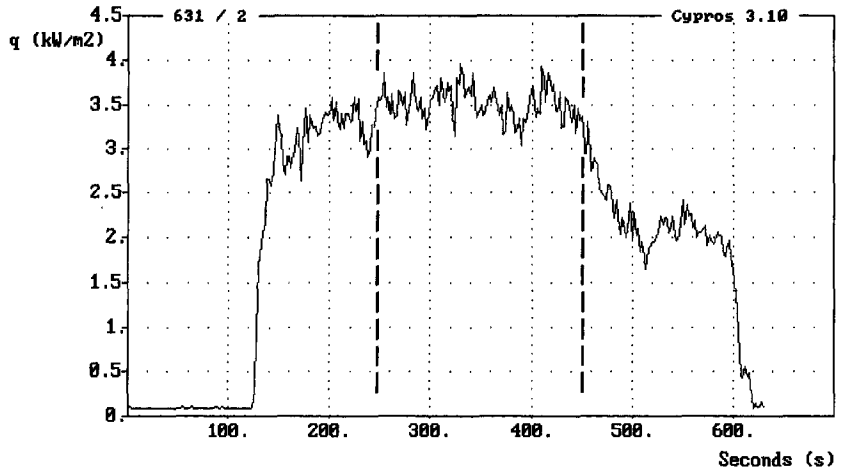

Fig. 2. Radiation heat flux measured in point 1 for measurement series MI (90 kg/s in marked interval).

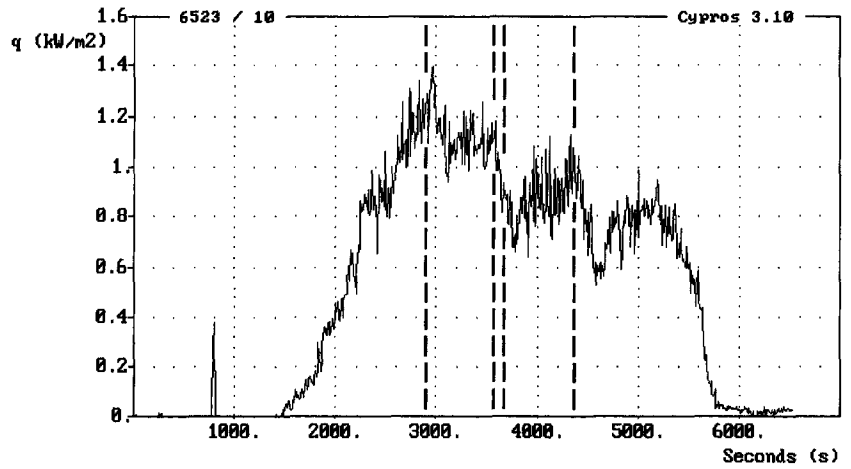

Fig. 3. Radiation heat flux measured in point 1 for measurement series MII (25.3 + 4.8 kg/s in first marked interval, 16 + 3 kg/s in second marked interval).

4. Comparison with empirical model calculations

4.1. Model description

The empirical model is equivalent to the model reported by Chamberlain [5] at Shell Thornton and is therefore called the Shell Thornton model here. The heat flux in

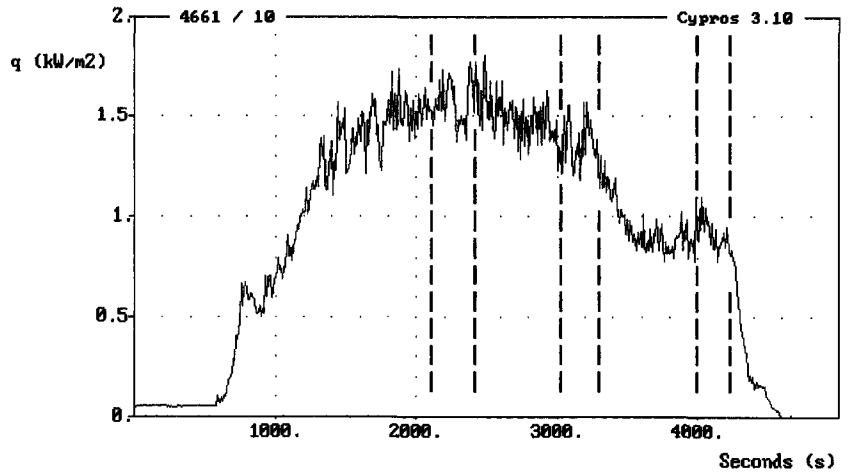

Fig. 4. Radiation heat flux measured in point 1 for measurement series MIII (44.8 kg/s in first marked interval, 31.4 kg/s in second marked interval and 16.9 kg/s in third marked interval).

Table 4
Comparison between measurements and calculations for series MI

Point #	Mass flow (kg/s)	$q''_{measured}$ (kW/m^2)	$q''_{stand.dev}$ (kW/m^2)	$q''_{calculated}$ (kW/m^2)	Deviation (%)	Distance to flame centre L (m)	Deviation including τ (%)
1	90.0	3.54	0.23	3.8	+7	136.3	−23
2		3.85	0.21	4.1	+7	137.7	−23
3		4.16	0.22	4.6	+11	132.1	−20
1	50.2	2.41	0.12	2.7	+12	132.1	−19
2		2.61	0.13	2.9	+11	134.2	−20
3		2.86	0.14	3.2	+12	128.6	−19

a point is given by [5]:

$$q'' = F_f \cdot F_s \frac{Q}{A_{fl}} \tau, \tag{2}$$

F_f is the view factor between a point and the flame assuming the flame is shaped like a truncated cone and the dimensions of the flame is calculated from an empirical expression of the flame area (A_{fl}) as a function mainly of outlet diameter and velocity and wind speed. F_s is the fraction of the heat developed (Q) that is lost as radiation to the surroundings and is a function of the outlet velocity only. This fraction is taken to be from 0.14 to 0.32 in the model and decreases with increasing outlet velocity. The absorbtion of the radiation from the flame by the surrounding air is taken care of by the transmissivity of the atmosphere τ. The transmissivity is assumed to be a function

Table 5
Comparison between measurements and calculations for series MII

Point #	Mass flow (kg/s)	$q''_{measured}$ (kW/m^2)	$q''_{stand.dev}$ (kW/m^2)	$q''_{calculated}$ (kW/m^2)	Deviation (%)	Distance to flame centre L (m)	Deviation including τ (%)
1	25.3 + 4.8	1.14	0.10	1.3	+14	134.2	−14
2		1.05	0.09	1.2	+14	144.2	−15
3		1.12	0.10	1.1	−2	133.5	−30
4		0.98	0.08	1.0	+2	146.9	−24
1	16.0 + 3.0	0.86	0.10	1.0	+16	131.2	−13
2		0.79	0.09	1.0	+27	141.2	−6
3		0.87	0.11	0.9	+3	130.7	−22
4		0.77	0.10	0.7	−9	144.3	−33

Table 6
Comparison between measurements and calculations for series MIII

Point #	Mass flow (kg/s)	$q''_{measured}$ (kW/m^2)	$q''_{stand.dev}$ (kW/m^2)	$q''_{calculated}$ (kW/m^2)	Deviation (%)	Distance to flame centre L (m)	Deviation including τ (%)
1	44.8	1.56	0.11	2.0	+28	132.8	−10
2		1.44	0.11	1.5	+4	135.3	−27
3		2.16	0.14	2.8	+30	125.9	−9
4		1.72	0.12	2.1	+22	147.6	−16
5		2.02	0.14	2.6	+29	140.9	−11
6		1.85	0.13	2.5	+35	141.9	−7
1	31.4	1.38	0.10	1.7	+23	128.1	−14
2		1.28	0.10	1.3	+2	130.5	−29
3		1.91	0.14	2.3	+20	121.2	−16
4		1.44	0.10	1.7	+18	143.4	−19
5		1.71	0.13	2.0	+17	136.8	−19
6		1.58	0.12	2.0	+27	138.0	−13
1	16.9	0.91	0.08	1.1	+21	124.2	−15
2		0.81	0.08	0.8	−1	126.8	−31
3		1.22	0.10	1.4	+15	118.1	−20
4		0.85	0.07	1.0	+18	141.4	−19
5		1.01	0.09	1.2	+19	135.2	−18
6		0.96	0.08	1.1	+15	135.6	−21

of the water vapour content of the air and is given by [8]:

$$\tau = 2.02 \cdot (P_w L)^{-0.09}, \tag{3}$$

where P_w is the water vapour pressure in Pa found from the air temperature and the relative humidity. L is the distance from the measurement point to the assumed flame centre obtained by the Shell Thornton model (see Tables 4–6). Eq. (3) is based on a flame temperature of 1500 K as in the Shell Thornton model [5].

4.2. Comparison between measurements and calculations

In Tables 4–6 the measurements are compared with calculations. First, the heat radiation levels were calculated without including the reduced transmissivity of the humid air. The result of these calculations shows that in most cases the flux is overestimated. However, this situation is changed when the absorbtion by the water vapour in the air is taken into consideration. The transmissivity of the air is reduced to 0.69–0.75 when absorbtion due to water vapour is included. This indicates that the Shell Thornton model gives conservative results as long as the transmissivity of the air is assumed to be unity.

Looking into the details, it is evident that point 3 and 4 in measurement series MII and point 2 in measurement series MIII have the largest discrepancy when measured values are compared with calculations incorporating the transmissivity of the air. These points are situated upstream of the flame and see the flame from behind. This is in accordance with the result of Chamberlain [5]. In measurement series MI, all the three points are looking at the flame from the side as is also the case for the points 1 and 2 in series measurement MII and points 1 and 4 in measurement series MIII. The rest of the points in measurement series MIII see the flame from ahead. It is not possible to detect any difference in agreement between measurements and calculations for points ahead of and beside the flame. The discrepancy is between -23% and -6%.

5. Conclusion

Measurements giving radiation heat flux data for large capacity flares at production oil/gas platforms and a gas processing plant has been obtained. These data are for simple low velocity pipe flares. The data are compared with calculations using the Shell Thornton model. The comparison shows that the Shell Thornton model tends to underestimate the radiation levels when the transmissivity of the air is included in the calculations. A more conservative result is obtained when the air is assumed to be dry. This could be looked upon as a worst-case situation and pre-calculation of radiation levels using the Shell Thornton model should assume 100% transmissivity. The best agreement between calculations and measurements are obtained for points beside and ahead of the flame, while calculations of the radiation level in points behind the flame show the largest discrepancy when compared with measurements.

Acknowledgements

The measurements on the two oil/gas platforms were performed together with Rolf Sørlie and together with Erling Mikkelsen on the gas processing plant. Their participation are gratefully acknowledged.

References

[1] Installation Guide, 3595 Series Isolated Measurement Pods, Schlumberger Technologies.
[2] Operating Manual, 35954A IMP/PC to S-net Adaptor, Schlumberger Technologies.
[3] Altair DOS Version Users Guide, Version 2.15, Dickinson Control Systems.
[4] Cypros Users Guide, Camo A/S.
[5] G..A. Chamberlain, Presented at the 4th Int. Flare System Seminar, 14–16 October, 1986, Trondheim.
[6] F.P. Incropera and D.P. DeWitt, Fundamentals of Heat and Mass Transfer, Wiley, New York, 3rd edn., 1990, pp. 414, 497.
[7] F.M. White, Viscous Fluid Flow, McGraw-Hill, New York, 1974, p. 502.
[8] Guidelines for Chemical Process Quantitative Risk Analysis, Centre for Chemical Process Safety of the American Institute of Chemical Engineers, 1989, p. 127.